Model for calculating effective temperature of exoplanet in low eccentricity binary star system. Calculating the effective temperature of Kepler-47b and Kepler-453b.

Musheghyan Emil

Abstract:

This study presents a model for calculating the effective temperature of exoplanets in low-eccentricity binary star systems, focusing on Kepler-47b and Kepler-453b. Existing models, typically designed for single-star systems, fail to account for the complexities of binary star dynamics. Our model incorporates key parameters such as stellar luminosities and planetary albedo, providing enhanced accuracy in estimating effective temperatures. We find that Kepler-47b has an effective temperature of approximately 452.56 K, while Kepler-453b is cooler at 251.72 K, indicating different thermal environments. These findings underscore the model's potential for advancing our understanding of planetary climates in binary systems.

Introduction:

The study of exoplanets has gained significant momentum in recent years, particularly with the advent of advanced observational techniques and space missions such as Kepler (Borucki et al., 2010). Among the myriad factors influencing the climate of exoplanets, effective temperature plays a crucial role. This parameter is determined by the balance between the energy received from the host stars and the energy radiated back into space, a balance complicated by the dynamics of binary star systems (Kopparapu et al., 2013).

This paper presents a model specifically designed to calculate the effective temperature of exoplanets in low-eccentricity binary star systems, focusing on two notable examples: Kepler-47b (Orosz et al., 2012) and Kepler-453b (Welsh et al., 2015b). Understanding these properties is essential for elucidating how binary star dynamics influence planetary climates. By employing a comprehensive approach that incorporates stellar luminosity, distance, and orbital mechanics, this model aims to deliver more accurate estimations of effective temperature, thereby enhancing our understanding of these intriguing worlds.

Through this research, we aim to contribute to the broader field of astrobiology and planetary science by elucidating the factors that govern the thermal environments of exoplanets in binary systems. The findings will not only deepen our comprehension of Kepler-47b and Kepler-453b but also serve as a foundation for future studies of exoplanets in similar configurations (Fressin et al., 2013).

Worked Systems:

In this study, we developed a model to calculate the effective temperatures of two specific exoplanets, Kepler-47b (Orosz et al., 2012) and Kepler-453b (Welsh et al., 2015b). The properties of both exoplanetary systems are detailed in Table 1.

Name	$M_1(M_\odot)$	$M_2(M_\odot)$	$R_1(R_\odot)$	$R_2(R_\odot)$	$T_1(K)$	$T_2(K)$	$a_s(A.U.)$	$a_p(A.U.)$
Kepler 453	0.944	0.1951	0.833	0.2150	5527	3226	0.18539	0.7903
Kepler 47	1.043	0.362	0.964	0.3506	5636	3357	0.0836	0.2956

Table 1: Properties of Kepler-453 (Welsh et al., 2015b) and Kepler-47 (Orosz et al., 2012).

Kepler-47b and Kepler-453b are both circumbinary, or P-type, exoplanets, characterized by low-eccentricity ($e < 0.1$) orbits around their central binary stars. Similarly, the binary star orbits within each system also exhibit low eccentricity. The eccentricities for each system are presented in Table 2.

Name	e_s	e_p
Kepler 453	0.0524	0.0359
Kepler 47	0.0234	0.035

Table 2: Eccentricities of Kepler-453 (Welsh et al., 2015b) and Kepler-47 (Orosz et al., 2012).

For our calculations, we assumed an Neptune albedo of 0.290, a standard value used in planetary temperature models for Neptune-like exoplanets.

Model:

Panet-stars configurations

Assuming that the planetary mass is negligible compared to the mass of each star, we derived an expression for the distances of the stars from the common center of mass.

$$r_1 = D\frac{M_2}{M_1 + M_2}$$

$$r_2 = D\frac{M_1}{M_1 + M_2}$$

The distance L and angle α are subsequently determined based on the schematic representation shown in Fig. 1.

$$L = D \left(\frac{R_1}{R_1 + R_2} - \frac{M_2}{M_1 + M_2} \right)$$

$$\sin \alpha = \frac{R_1 + R_2}{D}$$

The first configuration occurs when an observer on the planet views star B fully and star A only partially. This configuration is observed when the planet is positioned within the angular range [−β,β], where the angle β is illustrated in Fig. 2. Analyzing the triangle in Fig. 3 led to the following result:

$$\beta = \alpha - \arcsin \left[\left(\frac{R_1}{R_1 + R_2} - \frac{M_2}{M_1 + M_2} \right) \frac{R_1 + R_2}{a} \right]$$
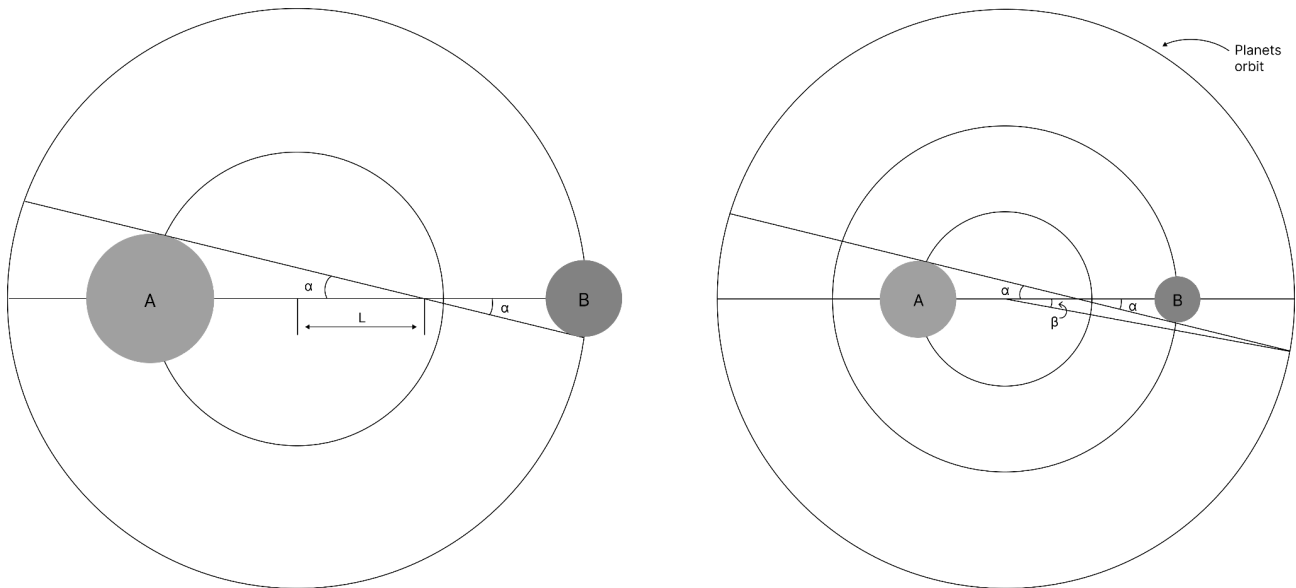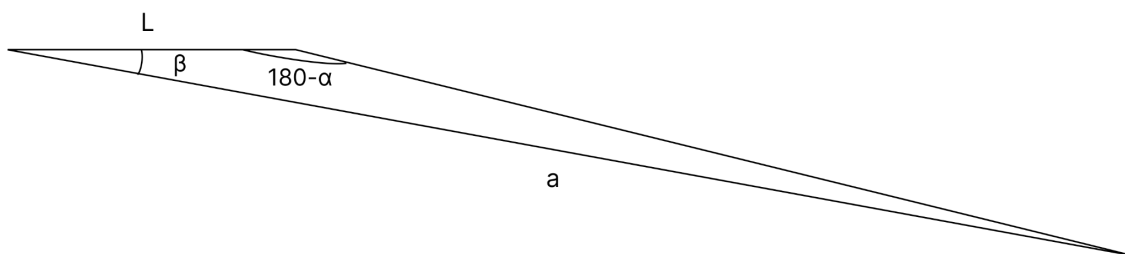

Figure 1,2

Figure 3

The second configuration occurs when an observer on the planet can fully view both star A and star B. This situation arises when the planet is positioned within the angular zones [β,µ]∪[−β,−µ], where the angle µ\muµ is illustrated in Fig. 4. Through analysis of the triangle depicted in Fig. 5, the following result was obtained:

$$
\mu = \arcsin\left[\left(\frac{R_1}{R_1 + R_2} - \frac{M_2}{M_1 + M_2}\right)\frac{R_1 + R_2}{a}\right] - \arcsin\left[\frac{R_1 + R_2}{D}\right]
$$

The third configuration occurs when an observer on the planet views star A fully, while star B is either partially visible or not visible at all. This configuration is observed within the angular range [µ,−µ]. Three distinct zones are identified, as shown in Fig. 6.
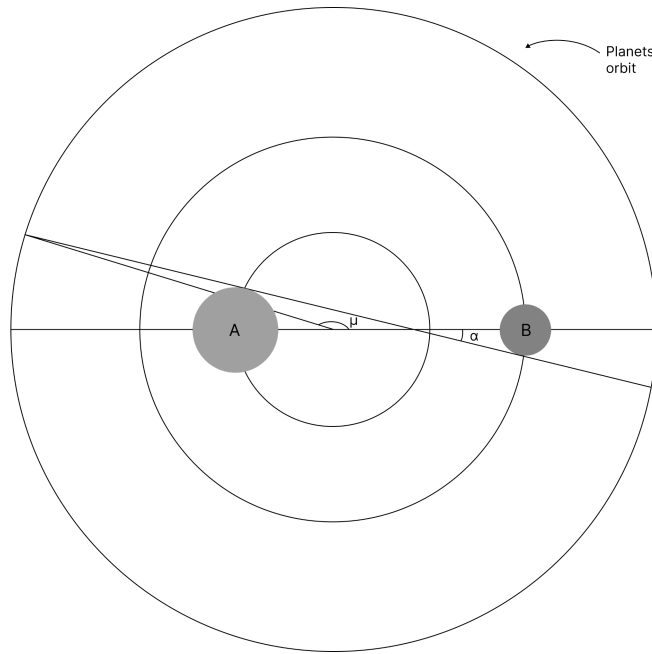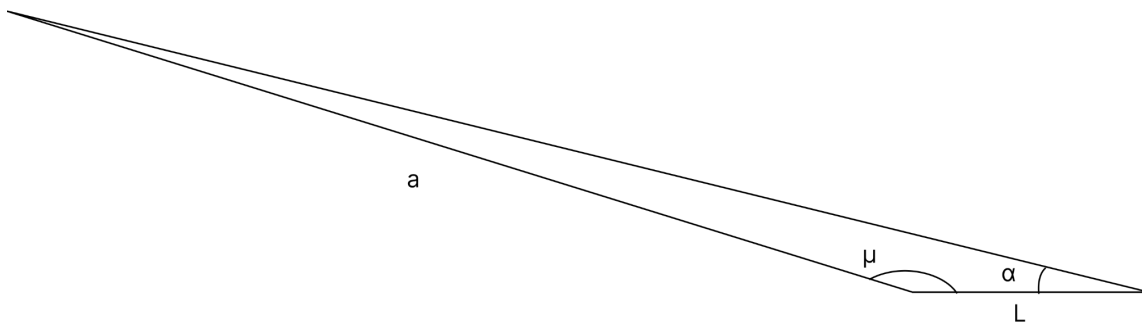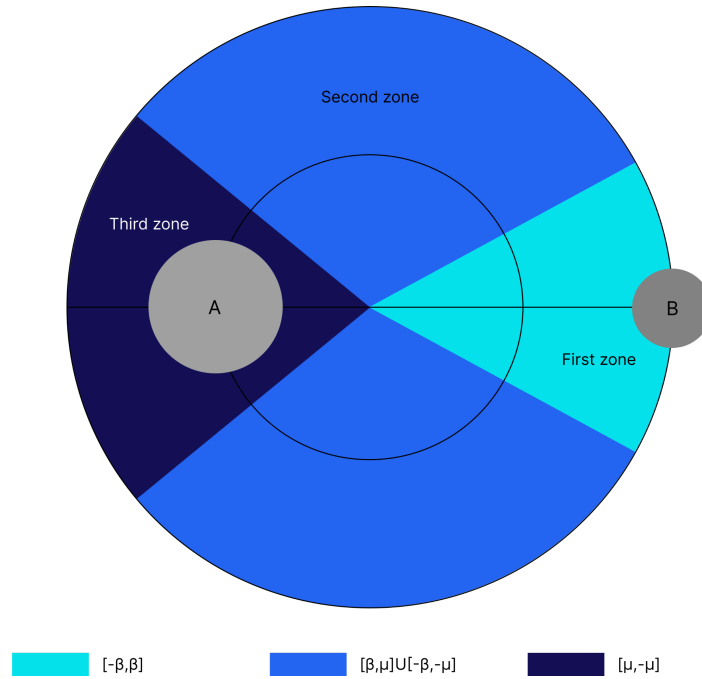

Figure 4

Figure 5

Figure 6

Distances of stars from the planet

To calculate the flux from the stars, it is essential to determine the distance between the stars and the planet as a function of the angular separation. We define X as the angle between the line connecting the star and the line connecting the planet to the center of mass.
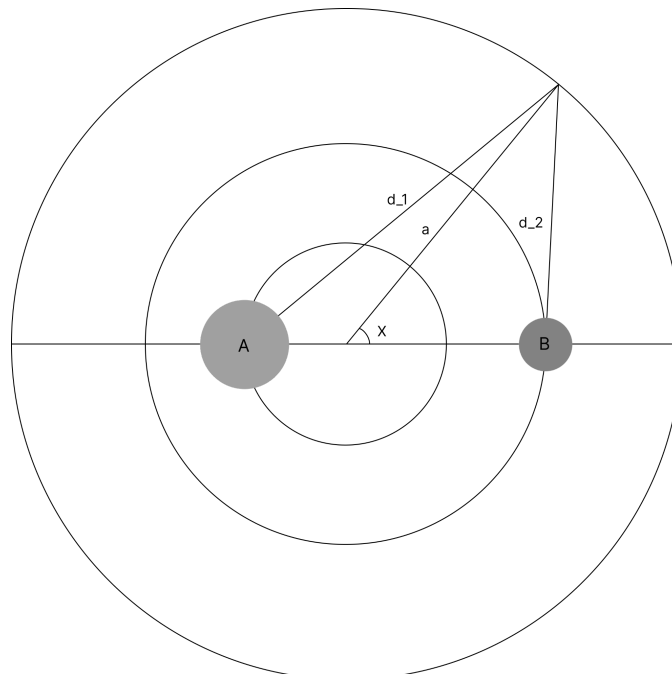

Figure 7

By applying the law of cosines to the triangles depicted in Figure 7, we obtain the following result:

$$d_1(x) = \sqrt{a^2 + D^2 \left(\frac{M_2}{M_1 + M_2}\right)^2 + 2aD\frac{M_2}{M_1 + M_2}\cos x}$$

$$d_2(x) = \sqrt{a^2 + D^2 \left(\frac{M_1}{M_1 + M_2}\right)^2 - 2aD\frac{M_1}{M_1 + M_2}\cos x}$$

Angular radiuses,distances, and areas of stars

We define θ_1 and θ_2 as the angular radii of the stars.

$$\theta_1 = \arctan\left[\frac{R_1}{d_1}\right]$$

$$\theta_2 = \arctan\left[\frac{R_2}{d_2}\right]$$

The diagram in Fig. 8 illustrates the angular separation between the centers of the stars as observed from the exoplanet, denoted as Ψ.
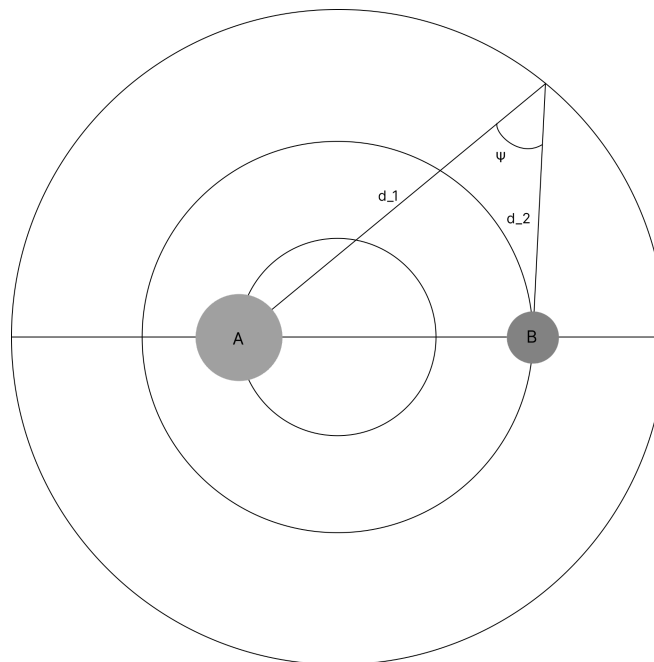

Figure 8

After solving the triangle shown in Figure 8, we obtain the following result:

$$\Psi = \arccos\left[\frac{d_1^2 + d_2^2 + D^2}{2d_1 d_2}\right]$$

A_1 and A_2 are the angular areas of stars.

$$A_1 = \pi\theta_1^2$$
$$A_2 = \pi\theta_2^2$$

Area of crossing section of stars during eclipse

During an eclipse, one star may overlap the other, causing a portion of one star to become obscured from the planet's perspective. We define the overlapped region as the area of intersection between the two stars. Using the formula for the area of overlapping circle (Jiménez et al., 2015), we get the following result.

$$A_{shaded} = Z_1 + Z_2 - Z_3$$

Where:

$$Z_1 = \theta_2^2\left(\frac{\Psi^2 + \theta_2^2 - \theta_1^2}{2\Psi\theta_2}\right)$$

$$Z_2 = \theta_1^2\left(\frac{\Psi^2 + \theta_1^2 - \theta_2^2}{2\Psi\theta_1}\right)$$

$$Z_3 = \frac{1}{2}\sqrt{(\theta_1 + \theta_2 - \Psi)(\Psi + \theta_2 - \theta_1)(\theta_1 + \Psi - \theta_2)(\theta_1 + \theta_2 + \Psi)}$$

Flux in each configuration

For calculating received energy in one period, we find an expression for flux in each configuration.

For x from 0 to β, if $\psi \leq \theta_1 - \theta_2$:

$$F_{1_1} = \frac{L_1}{4\pi d_1^2}\left(1 - \frac{A_{full_2}}{A_{full_1}}\right)$$

$$F_{2_1} = \frac{L_2}{4\pi d_2^2}$$

For x from 0 to β, if $\psi \geq \theta_1 - \theta_2$:

$$F_{1_1} = \frac{L_1}{4\pi d_1^2}\left(1 - \frac{A_{shaded}}{A_{full_1}}\right)$$

$$F_{2_1} = \frac{L_2}{4\pi d_2^2}$$

For x from β to μ:

$$F_{1_2} = \frac{L_1}{4\pi d_1^2}$$

$$F_{2_2} = \frac{L_2}{4\pi d_2^2}$$

For x from μ to π,if $\psi \geq \theta_1 - \theta_2$:

$$F_{1_3} = \frac{L_1}{4\pi d_1^2}$$

$$F_{2_3} = \frac{L_2}{4\pi d_2^2}\left(1 - \frac{A_{shaded}}{A_{full_2}}\right)$$

If $\psi \leq \theta_1 - \theta_2$:

$$F_{1_3} = \frac{L_1}{4\pi d_1^2}$$

$$F_{2_3} = 0$$

In all equations above flux is written with two indexes,F_{i_j}, i identifies the star (primary or secondary) and j identifies the zone (first, second or third).
Summary flux in each zone:

$$F_{\Sigma_j} = F_{1_j} + F_{2_j}$$

Where j identifies the zone.

$$F_{\Sigma_1} = F_{1_1} + F_{2_1}$$
$$F_{\Sigma_2} = F_{1_2} + F_{2_2}$$
$$F_{\Sigma_3} = F_{1_3} + F_{2_3}$$

Received energy in each configuration

I_i is the received energy divided by area of cross section of planet in each configuration:

$$I_i = \frac{W_i}{\pi R_{planet}^2}$$

W_i is the received energy in each configuration.

$$W_i = 2\int \frac{F_{\Sigma i}\pi R_{planet}^2}{\omega_{relative}}\,dx$$

$\omega_{relative}$, the relative angular speed of stars and planet, equals to:

$$\omega_{relative} = \sqrt{\frac{G(M_1 + M_2)}{D^3}} - \sqrt{\frac{G(M_1 + M_2)}{a^3}}$$

$$I_1 = 2\int_0^\beta \frac{F_{\Sigma_1}}{\omega_{relative}}\,dx$$

$$I_2 = 2\int_\beta^\mu \frac{F_{\Sigma_2}}{\omega_{relative}}\,dx$$

$$I_3 = 2\int_\mu^\pi \frac{F_{\Sigma_3}}{\omega_{relative}}\,dx$$

$$I_\Sigma = I_1 + I_2 + I_3$$

Thermal equilibrium

In formulating the condition for thermal equilibrium in this section, we have neglected the effects of the greenhouse phenomenon.

$$W_\Sigma(1 - A) = 4\pi R_{planet}^2 \sigma T^4 \frac{2\pi}{\omega_{relative}}$$

'A' represents the albedo of the exoplanet.

$$I_\Sigma(1 - A) = 8\sigma T^4 \frac{\pi}{\omega_{relative}}$$

$$T_{planet} = \left[\frac{I_\Sigma \omega_{relative}(1 - A)}{8\pi\sigma}\right]^{\frac{1}{4}}$$

Software

All calculations in this study were performed using Scilab (https://www.scilab.org/).

Results:

The results of the effective temperature (T_{eff}) calculations are presented in Table 3.

Name	$T_{eff}(K)$
Kepler-453b	251.72
Kepler-47b	452.56

Table 3: Calculated effective temperatures of Kepler-453b and Kepler-47b.

Discussion:

The effective temperatures calculated for Kepler-47b and Kepler-453b (452.56 K and 251.72 K, respectively) highlight the significant influence of dual stellar sources on planetary climates. The results from our model demonstrate that the unique configurations of binary star systems can

lead to distinct thermal environments, which is crucial for understanding the climate dynamics of these exoplanets.

Our model's ability to identify multiple planetary-star visibility configurations allows for a nuanced understanding of flux variability throughout the exoplanets' orbits (Doyle et al., 2011). This adaptability is particularly relevant in binary systems, where the contributions of each star to the total flux can vary dramatically based on the planet's orbital phase. Such an approach addresses limitations in existing models that often assume isotropic flux distributions or neglect complexities introduced by partial eclipses.

However, it is essential to acknowledge certain limitations of our model. For instance, the exclusion of atmospheric greenhouse effects may lead to an underestimation of surface temperatures, as these effects can significantly enhance temperatures on terrestrial planets. Future applications of this model would benefit from incorporating atmospheric dynamics, especially for exoplanets that may possess substantial atmospheres capable of retaining heat (Kopparapu et al., 2013). Moreover, while our model focuses on low-eccentricity binary systems, the findings suggest that higher eccentricity systems may exhibit greater thermal variations, warranting a tailored approach for such configurations (Dawson & Johnson, 2012).

From an astrobiological perspective, this study provides valuable insights into the climate of planets in binary star systems. The results for Kepler-47b and Kepler-453b underscore how stellar configuration impacts the thermal environments of these exoplanets, suggesting that the search for diverse planetary climates could confidently extend to similar binary systems (Fressin et al., 2013).

Future research should consider expanding this model to encompass a broader range of binary configurations, atmospheric models, and observational data from other Kepler-detected exoplanets in binary systems, refining predictions and enhancing our understanding of exoplanetary climates in diverse celestial arrangements.

Bibliography:

1. Borucki, W. J., Koch, D., Basri, G., Batalha, N., Brown, T., Caldwell, D., ... & Prsa, A. (2010). Kepler planet-detection mission: introduction and first results. Science, 327(5968), 977-980. https://doi.org/10.1126/science.1185402
2. Dawson, R. I., & Johnson, J. A. (2018). Origins of hot Jupiters. Annual Review of Astronomy and Astrophysics, 56(1), 175-221. https://doi.org/10.1146/annurev-astro-081817-051853
3. Doyle, L. R., Carter, J. A., Fabrycky, D. C., Slawson, R. W., Howell, S. B., Winn, J. N., ... & Fischer, D. (2011). Kepler-16: a transiting circumbinary planet. Science, 333(6049), 1602-1606. https://doi.org/10.1126/science.1210923

4. Fressin, F., Torres, G., Charbonneau, D., Bryson, S. T., Christiansen, J., Dressing, C. D., ... & Batalha, N. M. (2013). The false positive rate of Kepler and the occurrence of planets. The Astrophysical Journal, 766(2), 81. https://doi.org/10.1088/0004-637x/766/2/81

5. Jimenez, J., Gomez, A., Buhrmester, M. D., Vázquez, A., Whitehouse, H., & Swann, W. B. (2016). The dynamic identity fusion index. Social Science Computer Review, 34(2), 215-228. https://doi.org/10.1177/0894439314566178

6. Kopparapu, R. K., Ramirez, R., Kasting, J. F., Eymet, V., Robinson, T. D., Mahadevan, S., ... & Deshpande, R. (2013). Habitable zones around main-sequence stars: new estimates. The Astrophysical Journal, 765(2), 131. https://doi.org/10.1088/0004-637x/765/2/131

7. Orosz, J. A., Welsh, W. F., Carter, J. A., Fabrycky, D. C., Cochran, W. D., Endl, M., ... & Borucki, W. J. (2012). Kepler-47: a transiting circumbinary multiplanet system. Science, 337(6101), 1511-1514. https://doi.org/10.1126/science.1228380

8. Welsh, W. F., Orosz, J. A., Short, D. R., Cochran, W. D., Endl, M., Brugamyer, E., ... & Borucki, W. J. (2015). Kepler 453 b—the 10th Kepler transiting circumbinary planet. The Astrophysical Journal, 809(1), 26. https://doi.org/10.1088/0004-637x/809/1/26.